International Journal of Modern Physics B
Vol. 35, No. 19 (2021) 2150200 (8 pages)

DOI: 10.1142/S0217979221502003

Acid-based modified $NiCo_2O_4$ as high-performance supercapacitor electrode materials

Wenbo Geng*, Qing Wang*,†,‡, Jianfeng Dai*,† and Haoran Gao*

*School of Science, Lanzhou University of Technology, Lanzhou 730050, Gansu, P. R. China

†State Key Laboratory of Advanced Processing and Recycling of Non-Ferrous Metals, Lanzhou University of Technology, Lanzhou 730050, Gansu, P. R. China

‡wangqing@lut.edu.cn

Received 7 April 2021
Revised 25 May 2021
Accepted 3 June 2021
Published 29 July 2021

The performance of supercapacitor electrode materials was greatly affected by the specific surface area. The urchin-like $NiCo_2O_4$ was transformed into porous $NiCo_2O_4$ (AA-$NiCo_2O_4$) using the acid–alkali treatment method. The specific surface area of AA-$NiCo_2O_4$ was 165.0660 m^2/g, which was about three times larger than that of $NiCo_2O_4$. The specific capacitance of the AA-$NiCo_2O_4$ was enhanced significantly (1700 F/g at 1 A/g), and AA-$NiCo_2O_4$ possesses good rate capacitance (1277 F/g at 10 A/g). This is mainly attributed to the larger specific surface area, fast and convenient electron–ion transport and redox reaction. Therefore, AA-$NiCo_2O_4$ is a promising high-performance supercapacitor electrode material.

Keywords: Supercapacitor; $NiCo_2O_4$; hydrothermal synthesis; electrochemistry; crystal structure; energy storage and conversion.

PACS number: 82.45.Yz

1. Introduction

With the gradual depletion of traditional fossil energy sources, advanced green new energy storage devices of exploration have become the focus of current research.[1] As one type of latest electrochemical energy storage systems, supercapacitors have the advantages of fast charging speed, long cycle life, high-energy conversion efficiency and high power density,[2] which is considered as one of the most promising candidates for energy storage systems.[3]

‡Corresponding author.

Electrode materials play a vital role in the performance of supercapacitors. $NiCo_2O_4$ is currently a prevailing binary oxide in the field of power sources research.[4] Spinel-type $NiCo_2O_4$ exhibits superior electrochemical performance by utilizing a richer redox reaction between nickel and cobalt ions than single-component nickel oxide or cobalt oxide.[5–8] In addition, $NiCo_2O_4$ electrode materials can be used not only at the nanoscale, but also have various morphologies that show different electrochemical properties.[9,10] Therefore, $NiCo_2O_4$ has become a more promising and flexible alternative. In recent years, Shen *et al.*[11] developed a new and efficient self-template method for the preparation of uniform $NiCo_2O_4$ hollow spheres with a double-shell core structure. Li *et al.*[12] synthesized a one-dimensional (1D) $NiCo_2O_4$ nanotube (NCO-NTS) with a pore structure by electrospinning. The prepared NCO-NTS electrode showed a high specific capacitance of 1647 F/g at 1 A/g, and a capacity retention rate of 77.3% at 25 A/g. Zeng *et al.*[13] prepared $NiCo_2O_4$ by adding a template that showed different morphologies. $NiCo_2O_4$ electrodes using 0.75 g SDS, PVP and CTAB showed higher capacitance at 1 A/g, which were 1357, 1469 and 1290 F/g, respectively. Chen *et al.*[14] prepared $NiCo_2O_4$ nanosheets with the porous structure on nickel foam, the electrode material had a high specific capacitance (1734.9 F/g) at a current density of 2 A/g. Although the materials with better electrochemical performance are obtained by the above methods, the experimental process is more complicated. There are a large number of methods for preparing materials,[15–19] but it is very important to develop a simple method that can synthesize electrode materials with unique morphology and enhance the capacitive performance of nanostructured electrode materials.

At present, most researches focus on increasing the electrochemical performance by preparing porous electrode materials. This paper uses a simple and controllable method (acid–alkali treatment) to prepare porous $NiCo_2O_4$ electrode materials. The method is not only simple, easy to operate, high repetition rate, but also greatly improves the specific capacitance of $NiCo_2O_4$, the reason is that the porous structure can promote ion transport and electronic conduction for rapid redox reactions.

2. Experimental Procedures

2.1. *The synthesis of $NiCo_2O_4$*

1 mmol $NiCl_2 \cdot 6H_2O$ and 2 mmol $CoCl_2 \cdot 6H_2O$ were dissolved in a mixed solution of 20 mL H_2O and 20 mL ethanol at room-temperature. Then the solution was transferred to a stainless autoclave, the hydrothermal route was carried out by the addition of 15 mmol urea and heated to 120°C for 8 h. Next, the $NiCo_2(OH)_6$ precursors were collected and cleaned several times with deionized water and ethanol, and dried at 60°C for 6 h. Finally, the urchin-like $NiCo_2O_4$ was obtained by annealing treatment at 350°C for 3 h. The formation process of $NiCo_2O_4$ was as follows[20]:

$$6CO(NH_2)_2 \rightarrow C_3H_6N_6 + 6NH_3 + 3CO_2, \quad (1)$$

$$NH_3 + H_2O \rightarrow NH_4^+ + OH^-, \quad (2)$$

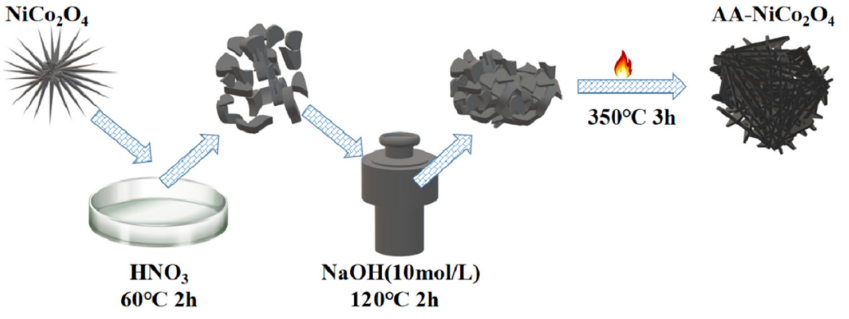

Fig. 1. (Color online) Schematic illustration of the synthesis process of the AA-$NiCo_2O_4$.

$$Ni^{2+} + 2Co^{2+} + 6OH^- \rightarrow NiCo_2(OH)_6, \tag{3}$$

$$NiCo_2(OH)_6 + 1/2O_2 \rightarrow NiCo_2O_4 + 3H_2O. \tag{4}$$

2.2. *The synthesis of AA-$NiCo_2O_4$*

A schematic illustration of the synthesis process of the AA-$NiCo_2O_4$ is shown in Fig. 1, $NiCo_2O_4$ was treated with concentrated HNO_3 at 60°C for 2 h, the acidified samples were transferred into a 50 mL autoclave. Then the NaOH solution ($10\ mol \cdot L^{-1}$) was added into the autoclave that was kept at 120°C for 2 h. Afterward, the obtained samples were cleaned thoroughly with deionized water and ethanol, and dried at 60°C for 12 h. Finally, AA-$NiCo_2O_4$ was fabricated in the same thermal environment.

2.3. *Characterization*

X-ray diffraction (XRD) spectrometer equipped with CuKα radiation was explored to investigate the phase structures of the materials. Scanning electron microscope (SEM, JSM-6700F) and transmission electron microscope (TEM, JEM-2010) were employed to explore the morphologies of the materials. Nitrogen adsorption–desorption (ASAP2020) was applied to examine the specific surface areas and the pore structure of the samples.

2.4. *Electrochemical measurements*

The 1×2 cm nickel foam was treated with HCl, acetone and deionized water, respectively, and ultrasound for 30 min. The electrochemically active materials, PVDF (binder) and acetylene carbon black (conducting agent), were mixed at a mass ratio of 8:1:1 and uniformly coated on a nickel foam plate of 1×2 cm, and then dried at 60°C for 24 h, the mass load of the electrode was about 2 $mg \cdot cm^2$. The electrochemical performance was studied in a three-compartment battery using a 5 M KOH aqueous solution as the electrolyte. A mercury electrode was used as the

reference electrode, and a platinum mesh was used as the counter electrode. The specific capacities were calculated according to the following equation:

$$C = \frac{I \times \Delta t}{m}, \tag{5}$$

where I refers to the constant discharge current, Δt represents the discharge time, m is the corresponding active materials mass.

3. Results and Discussion

As shown in Fig. 2(a), two samples exhibited identical phase structure of spinel-type nickel–cobalt ore ($NiCo_2O_4$). The major diffraction peaks observed at $2\theta = 18.906°$, 31.148°, 36.696°, 38.404°, 44.622°, 55.439°, 59.094°, 64.980° and 68.309° belonged to the (111), (220), (311), (222), (400), (422), (511), (440) and (531) planes of spinel-type nickel–cobalt ore ($NiCo_2O_4$) (PDF#20-0781), respectively. Compared with $NiCo_2O_4$, the AA-$NiCo_2O_4$ sample showed a better crystallization degree. This could be due to the re-calcination process at a high-temperature which could promote the process of crystallization.

According to the high-resolution TEM (HRTEM) image in Fig. 2(b), the lattice fringes with spacing was measured to be 0.234 nm, corresponding to the (222) crystal plane of AA-$NiCo_2O_4$. In addition, the well-defined diffraction rings are shown in the selected area electron diffraction (SAED) pattern [Fig. 2(c)] to indicate the polycrystalline nature of AA-$NiCo_2O_4$.

Figure 3 recorded the morphology changes of samples during the acid–alkali etching process. Figure 3(a) shows the SEM image of $NiCo_2O_4$, displaying an urchin-like structure. The SEM image of the sample after concentrated nitric acid treatment is shown in Fig. 3(b). It illustrates the surface of the sample etched by acid, and the generation of many flake particles whose size was between 30 and 100 nm could be seen clearly due to the exfoliation of $NiCo_2O_4$ on the surface. The SEM image of alkalized $NiCo_2O_4$ after acidification is shown in Fig. 3(c). The alkali treatment process contributed to the regrowth of acidified $NiCo_2O_4$ which accumulated flake particles to form a porous material. Figure 3(d) shows a SEM image of the AA-$NiCo_2O_4$, it could be clearly seen that the sample presents a porous structure.

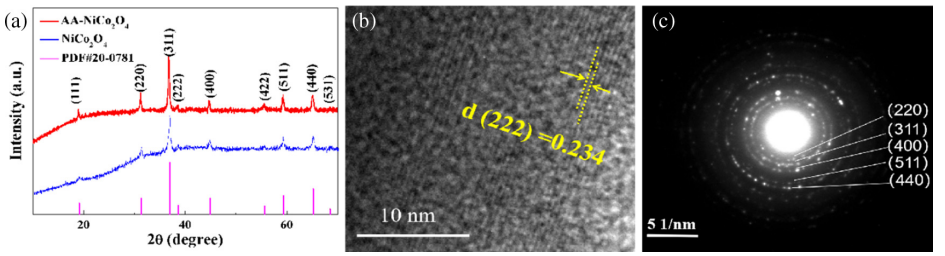

Fig. 2. (Color online) (a) XRD pattern of the $NiCo_2O_4$ and AA-$NiCo_2O_4$; (b) HRTEM image of AA-$NiCo_2O_4$; (c) SAED pattern of the AA-$NiCo_2O_4$.

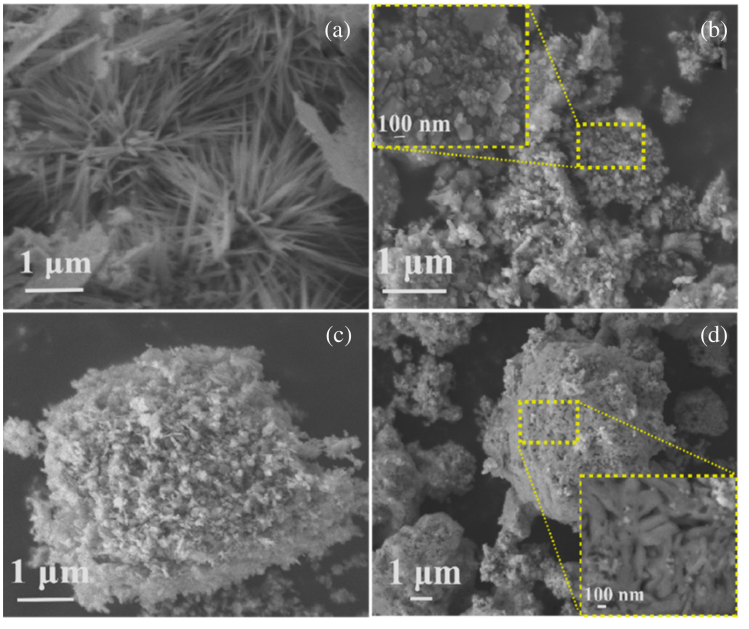

Fig. 3. (Color online) SEM image of (a) $NiCo_2O_4$; (b) acidified $NiCo_2O_4$; (c) alkalized $NiCo_2O_4$ after acidified; (d) AA-$NiCo_2O_4$.

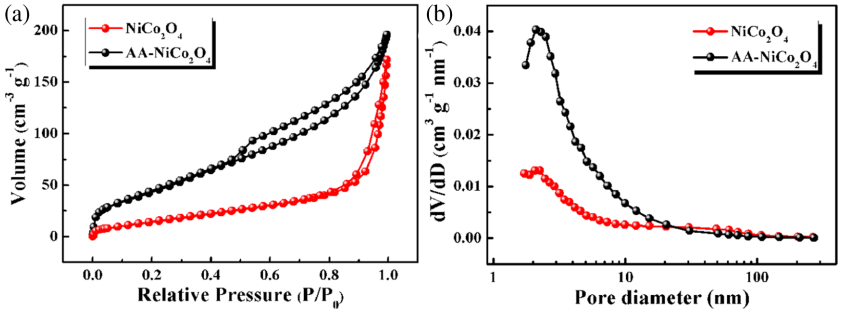

Fig. 4. (Color online) (a) N_2 adsorption–desorption isotherm; (b) pore size distribution of $NiCo_2O_4$ and AA-$NiCo_2O_4$.

As shown in Fig. 4(a), two samples display type IV isotherm and typical H3 hysteresis loop with the characteristic of mesoporous structures. The H3 hysteresis loop could be considered as a slit hole formed by the accumulation of lamellar particles, which is consistent with Figs. 3(c) and 3(d).

The aperture distribution diagram confirms that AA-$NiCo_2O_4$ had clear micropores and mesopores and that the aperture distribution was more concentrated than $NiCo_2O_4$ [Fig. 4(b)]. The average pore size of AA-$NiCo_2O_4$ is 7.09 nm, the average pore size of $NiCo_2O_4$ is 16.18 nm. Unique porous nature facilitates ion diffusion to promote effectively the electrochemical reaction. The specific surface area

was determined by Brunauer–Emmett–Teller analysis. The specific surface area of AA-$NiCo_2O_4$ was found to be 165.0660 m^2/g, about three times that of $NiCo_2O_4$ (56.4880 m^2/g). The increase of the specific surface area facilitates rapid ions transport and ensures adequate contact between the electrolytes and electrode materials, and further improved the electrochemical performance of electrode materials.

In a three-electrode system, the electrochemical properties of the material were measured by cyclic voltammetry (CV), galvanostatic charge–discharge (GCD) and electrochemical impedance spectroscopy (EIS). As shown in Figs. 5(a) and 5(b), both the CV curves possess a pair of redox peaks, which were characteristic of a Faraday redox reaction behavior. The corresponding reaction occurring in the working process could be expressed in the following equations[21]:

$$NiCo_2O_4 + OH^- = NiOOH + 2CoOOH + e^-, \tag{6}$$

$$CoOOH/NiOOH + OH^- = CoO_2/NiO_2 + H_2O + e^-. \tag{7}$$

Next, we compared the electrochemical properties of the two materials. Figure 5(c) shows the CV curves of the two samples at 20 mV/s. AA-$NiCo_2O_4$ possesses a larger area of the closed curve, which means it has a higher capacity value.

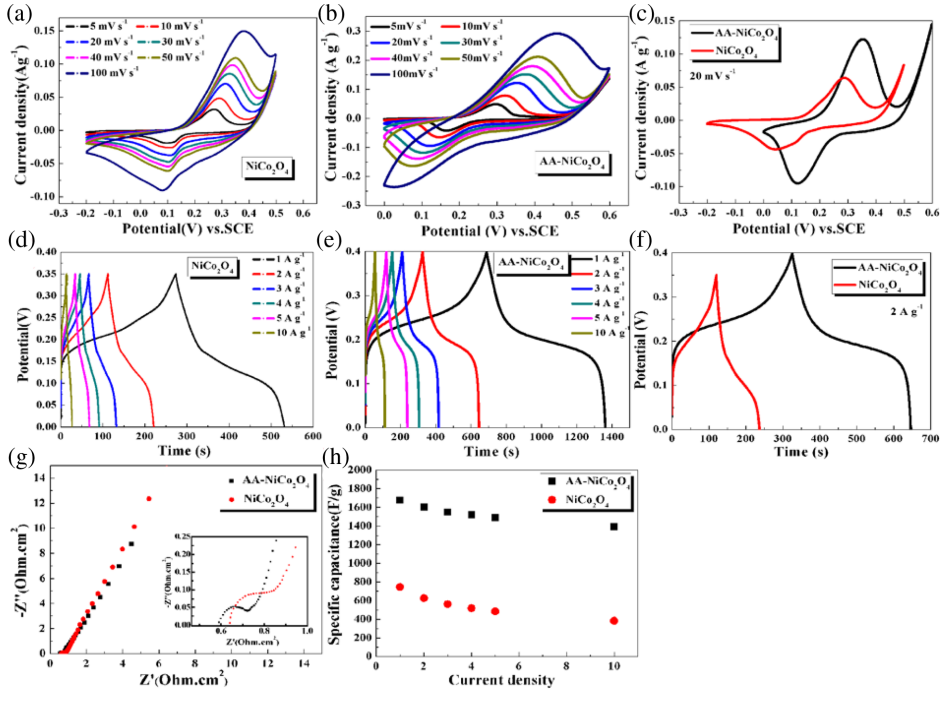

Fig. 5. (Color online) CV curves (a) $NiCo_2O_4$, (b) AA-$NiCo_2O_4$, (c) comparison among $NiCo_2O_4$ and AA-$NiCo_2O_4$; GCD curves (d) $NiCo_2O_4$, (e) AA-$NiCo_2O_4$; (f) comparison among $NiCo_2O_4$ and AA-$NiCo_2O_4$; (g) EIS comparison among $NiCo_2O_4$ and AA-$NiCo_2O_4$; (h) rate capability comparison among $NiCo_2O_4$ and AA-$NiCo_2O_4$.

To determine the specific capacitance of the electrode, continuous current charge–discharge measurements were performed over a voltage range of 0–0.4 V [Figs. 5(d) and 5(e)]. The GCD curves of the two materials exhibited different stationary periods, indicating the Faraday reaction had occurred, which were consistent with the CV measurements. Besides, the GCD curves were almost symmetrical, indicating that the Faraday redox reaction had great reversibility. Figure 5(f) shows a comparison of the GCD curves of the two samples at 2 A/g, AA-$NiCo_2O_4$ possesses a longer discharge time, thus a higher specific capacity, because AA-$NiCo_2O_4$ also possesses a larger specific surface area than $NiCo_2O_4$.

As shown in Fig. 5(g), in the high-frequency region, the semicircle diameter of AA-$NiCo_2O_4$ was significantly smaller than that of $NiCo_2O_4$, indicating that the charge transfer impedance of AA-$NiCo_2O_4$ was small, which meant that AA-$NiCo_2O_4$ still possessed better electrochemical performance at high current densities. Therefore, it showed that the rate performance of AA-$NiCo_2O_4$ is better. Through the curve fitting, the internal resistance (R_s) of $NiCo_2O_4$ and AA-$NiCo_2O_4$ samples was 0.62 and 0.58 Ω, respectively, and the charge transfer resistance (R_{ct}) of $NiCo_2O_4$ and AA-$NiCo_2O_4$ samples was 0.76 and 0.064 Ω, respectively, which further showed the internal resistance of the AA-$NiCo_2O_4$ sample was smaller, the charge migration rate was faster, and it reflected excellent electrochemical performance. The specific capacitances at various current densities are shown in Fig. 5(h). The AA-$NiCo_2O_4$ electrode provided high specific capacitances of 1700.0, 1601.1, 1553.9, 1517.7, 1486.5 and 1277.5 F/g at current densities of 1, 2, 3, 4, 5 and 10 A/g, respectively. When the current density was increased from 1 to 10 A/g, approximately 75% of the specific capacitance was retained, which also proves that AA-$NiCo_2O_4$ possessed good rate performance. This was attributed to the special porous structure of $NiCo_2O_4$, which provided a relatively stable structure so that $NiCo_2O_4$ could still possess good electrochemical performance at a larger current density.

4. Conclusions

In summary, porous $NiCo_2O_4$ with high specific capacitance had been prepared by a simple acid–alkali treatment method. After acid-based treatment, a porous structure material is obtained, and the specific capacitance of the material is greatly improved. The specific capacitance was increased from 750 to 1700 F/g at 1 A/g, due to this, the structure provided a larger specific surface area, which was conducive to the transport of ions and produces a more adequate reaction. AA-$NiCo_2O_4$ also has excellent rate performance, when it is increased to 10 A/g, it can still retain a specific capacitance of about 75%. Therefore, acid–alkali-treated $NiCo_2O_4$ was a supercapacitor electrode material with excellent electrochemical performance, and acid-based treatment was an effective method to improve the electrochemical performance of electrode materials.

Acknowledgments

The authors are highly grateful for the support offered by the National Nature Science Foundation of China (No. 11664023) and State Key Laboratory of Advanced Processing and Recycling of Non-Ferrous Metals.

References

1. Z. Yang *et al.*, *Chem. Rev.* **111**, 3577 (2011).
2. C. Zhao, J. Zhu, Y. Jiang *et al.*, *Mater. Lett.* **271**, 127799 (2020).
3. Y. Zhu *et al.*, *Electrochim. Acta* **269**, 30 (2018).
4. Q. Zhou *et al.*, *J. Electrochem. Soc.* **161**, A1922 (2014).
5. L. Yu *et al.*, *Chem. Commun.* **49**, 137 (2013).
6. L. Q. Mai *et al.*, *Nat. Commun.* **2**, 1 (2011).
7. M. C. Liu *et al.*, *J. Mater. Chem. A* **1**, 1380 (2013).
8. Q. Wang *et al.*, *J. Mater. Chem.* **22**, 21647 (2012).
9. J. Liu and X. W. Liu, *Adv. Mater.* **24**, 4097 (2012).
10. G. Zhang and X. W. D. Lou, *Sci. Rep.* **3**, 1 (2013).
11. L. Shen *et al.*, *Angew. Chem., Int. Ed.* **54**, 1868 (2015).
12. L. Li *et al.*, *Chem. Eur. J.* **19**, 5892 (2013).
13. Z. Zeng *et al.*, *Ionics* **25**, 2791 (2019).
14. X. Chen *et al.*, *Sci. Rep.* **10**, 1 (2020).
15. L. Arun *et al.*, *J. Mater. Sci., Mater. Electron.* **29**, 21180 (2018).
16. C. Karthikeyan *et al.*, *J. Mater. Sci., Mater. Electron.* **30**, 8097 (2019).
17. E. Elanthamilan *et al.*, *Sustain. Energy Fuels* **2**, 811 (2018).
18. L. Arun *et al.*, *J. Phys. Chem. Solids* **136**, 109155 (2020).
19. X. Shi *et al.*, *Nano* **15**, 2050149 (2020).
20. Z. Wang *et al.*, *J. Colloid Interface Sci.* **460**, 303 (2015).
21. J. S. Wei *et al.*, *Small* **12**, 5927 (2016).